Jelle Vriend*, Charlotte A. Hoogstraten, Kevin R. Venrooij, Bartholomeus T. van den Berge, Larissa P. Govers, Arno van Rooij, Marleen C.D.G. Huigen, Tom J.J. Schirris, Frans G.M. Russel, Rosalinde Masereeuw and Martijn J. Wilmer

Organic anion transporters 1 and 3 influence cellular energy metabolism in renal proximal tubule cells

https://doi.org/10.1515/hsz-2018-0446
Received November 30, 2018; accepted December 29, 2018; previously published online January 17, 2019

Abstract: Organic anion transporters (OATs) 1 and 3 are, besides being uptake transporters, key in several cellular metabolic pathways. The underlying mechanisms are largely unknown. Hence, we used human conditionally immortalized proximal tubule epithelial cells (ciPTEC) overexpressing OAT1 or OAT3 to gain insight into these mechanisms. In ciPTEC-OAT1 and -OAT3, extracellular lactate levels were decreased (by 77% and 71%, respectively), while intracellular ATP levels remained unchanged, suggesting a shift towards an oxidative phenotype upon OAT1 or OAT3 overexpression. This was confirmed by increased respiration of ciPTEC-OAT1 and -OAT3 (1.4-fold), a decreased sensitivity to respiratory inhibition, and characterized by a higher demand on mitochondrial oxidative capacity. In-depth profiling of tricarboxylic acid (TCA) cycle metabolites revealed reduced levels of intermediates converging into α-ketoglutarate in ciPTEC-OAT1 and -OAT3, which via 2-hydroxyglutarate metabolism explains the increased respiration. These interactions with TCA cycle metabolites were in agreement with metabolomic network modeling studies published earlier. Further studies using OAT or oxidative phosphorylation (OXPHOS) inhibitors confirmed our idea that OATs are responsible for increased use and synthesis of α-ketoglutarate. In conclusion, our results indicate an increased α-ketoglutarate efflux by OAT1 and OAT3, resulting in a metabolic shift towards an oxidative phenotype.

Keywords: α-ketoglutarate; cellular energy metabolism; OAT1; OAT3; renal proximal tubule epithelial cells; TCA cycle.

***Corresponding author: Jelle Vriend,** Department of Pharmacology and Toxicology, Radboud Institute for Molecular Life Sciences, Radboud University Medical Center, P.O. Box 9101, NL-6500HB, Nijmegen, The Netherlands, e-mail: jelle.vriend@radboudumc.nl
Charlotte A. Hoogstraten, Tom J.J. Schirris and Frans G.M. Russel: Department of Pharmacology and Toxicology, Radboud Institute for Molecular Life Sciences, Radboud University Medical Center, P.O. Box 9101, NL-6500HB, Nijmegen, The Netherlands; and Centre for Systems Biology and Bioenergetics, Radboud Center for Mitochondrial Medicine, Radboud University Medical Center, P.O. Box 9101, NL-6500HB, Nijmegen, The Netherlands
Kevin R. Venrooij, Bartholomeus T. van den Berge, Larissa P. Govers and Martijn J. Wilmer: Department of Pharmacology and Toxicology, Radboud Institute for Molecular Life Sciences, Radboud University Medical Center, P.O. Box 9101, NL-6500HB, Nijmegen, The Netherlands
Arno van Rooij and Marleen C.D.G. Huigen: Department of Laboratory Medicine, Translational Metabolic Laboratory (TML), Radboud University Medical Center, P.O. Box 9101, NL-6500HB, Nijmegen, The Netherlands
Rosalinde Masereeuw: Division of Pharmacology, Utrecht Institute for Pharmaceutical Sciences, Universiteitsweg 99, NL-3584CG, Utrecht, The Netherlands

Introduction

Renal excretion of organic anions is mainly mediated via organic anion transporters 1 and 3 (OAT1, *SLC22A6*; and OAT3, *SLC22A8*), both members of the solute carrier 22 (SLC22) subfamily of membrane transporters, that are localized to the basolateral side of proximal tubule epithelial cells (PTEC). OAT1 and OAT3 share common endogenous and exogenous substrates, while some differences in substrate affinity have been found. In general, OAT1 translocates smaller organic anions while OAT3 handles bulkier and more hydrophobic substrates (Eraly et al., 2006; Wikoff et al., 2011; Wu et al., 2013, 2017; Bush et al., 2017).

To fulfill the high ATP demand required for active uptake and efflux of various endogenous and exogenous compounds, renal proximal tubular cells are rich in mitochondria that tightly control their energetic state (O'Connor, 2006; Pagliarini et al., 2008). ATP is mainly produced via the tricarboxylic acid (TCA) cycle and oxidative phosphorylation (OXPHOS), a process that is executed by the concerted action of five multiprotein complexes. Complex I to IV are part of the electron transport system (ETS) and complex V functions as ATP synthase.

OAT1 and OAT3 are antiporters that mediate organic anion uptake in exchange for intracellular dicarboxylates, in particular the TCA cycle metabolite α-ketoglutarate (Shimada et al., 1987; Pritchard, 1988; Kaufhold et al., 2011). Dicarboxylates are derived from intracellular pools and via extracellular uptake through the sodium-dicarboxylate co-transporter 3 (NaDC3, *SLC13A3*). In turn, NaDC3 is dependent on the sodium-potassium gradient maintained by Na^+,K^+-ATPase. In agreement with the close connection between TCA cycle metabolites and OAT function, inhibition of mitochondrial complex III by antimycin A and the consequent depletion of intracellular levels of α-ketoglutarate, resulted in decreased uptake of p-aminohippurate (PAH), a prototypical organic anion, in opossum kidney (OK) PTEC (Nagai et al., 1998).

To investigate further the relation between OAT1 and cellular metabolism, whole body oxygen consumption and CO_2 production was measured in Oat1-deficient mice, but no differences were observed (Eraly et al., 2006). These mice did, however, demonstrate higher urinary concentrations for α-ketoglutarate. Metabolic network-based predictions using transcriptomic and metabolomic data of these mice suggested a central role of OAT1 in several metabolic pathways, including the TCA cycle, and the biosynthesis of amino acids, fatty acids, prostaglandins, cyclic nucleotides, and vitamins (Ahn et al., 2011; Liu et al., 2016). While this suggests a strong link between OAT1 and energy metabolism in PTEC, this association is less clear for OAT3, which appears to be important in systemic metabolism modulating metabolite levels of flavonoids and bile acids (Bush et al., 2017). These metabolomics and pathway analyses in knockout models proposed an important role of OAT1 and OAT3 in metabolic pathways, besides their pivotal role in xenobiotics transport.

Recently, human conditionally immortalized PTEC (ciPTEC) models overexpressing OAT1 (ciPTEC-OAT1) or OAT3 (ciPTEC-OAT3) have been established (Wilmer et al., 2010; Nieskens et al., 2016). Stable expression and function have been demonstrated, as well as their use in nephrotoxicity screening (Nieskens et al., 2016; Fedecostante et al., 2018; Suter-Dick et al., 2018; Vriend et al., 2018). The availability of these cellular models now allows investigation of the direct effects both transporters exert on mitochondrial function. Therefore, this study aims to compare OXPHOS-mediated energy metabolism in ciPTEC-OAT1 and -OAT3 with ciPTEC-parent, used as isogenic controls, and to examine the correlation between levels of TCA cycle metabolites and organic transport activity *in vitro*. Hence, we expect to provide enhanced mechanistic insight into the proposed link between OAT1 and OAT3 and energy metabolism.

Results

To examine the effects of OAT1 and OAT3 on the cellular metabolic phenotypes, we first determined intracellular ATP and extracellular lactate concentrations. Intracellular ATP levels, measured in fully matured monolayers of all three cell lines, were found to be comparable (Figure 1A). Extracellular lactate levels were, however, significantly decreased in ciPTEC-OAT1 and -OAT3 compared to ciPTEC-parent by 77 ± 7% and 71 ± 3%, respectively (Figure 1B), suggesting decreased glycolytic activity. Under glycolytic conditions, intracellular pyruvate levels can increase and be converted via lactate dehydrogenase (LDH) to lactate, which is subsequently excreted from the cell. To further investigate such a shift of the cellular metabolic phenotype from the glycolytic phenotype in ciPTEC-OAT1 and -OAT3, we measured basal oxygen consumption, corrected for non-cellular respiration (Figure 1C). The observed increased respiratory rates in ciPTEC-OAT1 and -OAT3 (both 1.4 ± 0.1-fold) as compared to ciPTEC-parent (Figure 1C), is in line with the idea that metabolism is shifted towards a more oxidative phenotype.

This increased oxidative phenotype was investigated further upon exposure to antimycin A, a known inhibitor of OXPHOS complex III (Brandt et al., 1988). No significant differences were observed in response to OXPHOS-inhibition by antimycin A, as demonstrated by similar IC_{50} values (Table S1). Either direct (10 nM) or prolonged (10 nM, 24 h) exposure to antimycin A was sufficient to fully inhibit cellular respiration in all three cell lines (Figure S1A, B), which is in line with earlier observations in ciPTEC-parent (Peters et al., 2017). To exclude any cytotoxic effects of the prolonged antimycin A exposure, we assessed cell viability after a 24-h exposure to a 1000-times higher antimycin A (10 μM) concentration. Cell viability was comparable to vehicle and thus no cytotoxic effects were expected up to 10 μM antimycin A (Figure S1C). To confirm inhibition of cellular respiration upon antimycin A exposure, gene expression of hypoxia-inducible factor 1-alpha (HIF1α) was measured, which was strongly upregulated after a 24-h exposure to 10 nM antimycin A in all cell lines (Figure S1D).

Next, we used this antimycin A-inhibited state, in which the contribution of cellular respiration is excluded, to get a better understanding of the mechanism by which OAT1 and OAT3 affect the metabolic phenotype. All three cell lines were exposed to antimycin A (0.05–15 nM, 24 h), which dose-dependently decreased ATP levels (66 ± 11%) compared to vehicle at concentrations starting from 5 nM in ciPTEC-parent (Figure 1D). In contrast, ATP levels in ciPTEC-OAT1 and -OAT3 remained

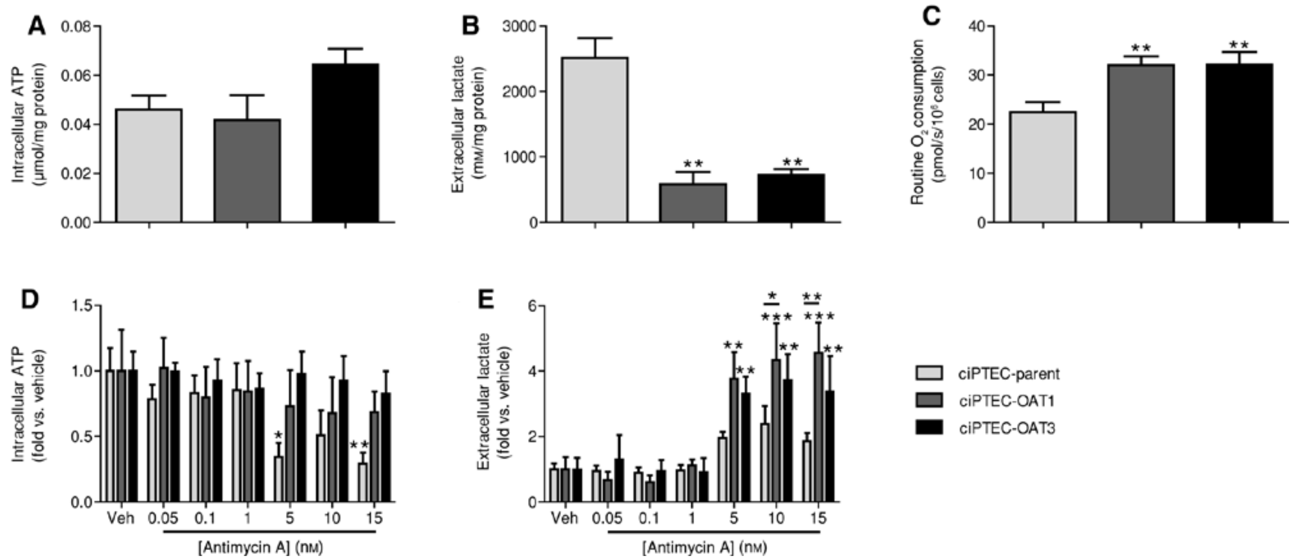

Figure 1: Overexpression of OAT1 and OAT3 resulted in a more oxidative phenotype.
(A) Total levels of intracellular ATP and (B) extracellular lactate, as measure for glycolytic activity, in ciPTEC-parent, -OAT1 and -OAT3. (C) Basal oxygen consumption, corrected for non-cellular respiration, was increased in ciPTEC-OAT1 and -OAT3, suggesting a shift of cellular metabolic phenotype from a glycolytic towards a more oxidative phenotype. Upon exposure to antimycin A (0.05–15 nм, 24 h), (D) normalized levels of intracellular ATP decreased in ciPTEC-parent, but not in ciPTEC-OAT1 and -OAT3. (E) Extracellular levels of lactate were strongly increased in ciPTEC-OAT1 and -OAT3. Statistical analysis for cell line comparison (A, B and C): $^{**}p < 0.01$ compared to ciPTEC-parent. Statistical analysis for antimycin A exposure (D and E), significant differences of means were compared using two-way ANOVA followed by Bonferroni's post-hoc tests, unless indicated otherwise: $^{*}p < 0.05$ compared to corresponding vehicle, $^{**}p < 0.01$ compared to corresponding vehicle, $^{***}p < 0.001$ compared to corresponding vehicle.

largely similar compared to vehicle (Figure 1D). In addition, lactate levels increased upon exposure to antimycin A, indicating a shift towards anaerobic metabolism (Figure 1E). At 5 nм antimycin A, this increase in lactate was, however, highly elevated in ciPTEC-OAT1 and -OAT3 compared to vehicle (3.8 ± 0.8-fold and 3.3 ± 0.5-fold, respectively) and less in ciPTEC-parent (2.0 ± 0.2-fold). The combination of stable ATP levels and increased lactate levels could be indicative of a compensatory increase of the glycolytic flux as observed previously (Liemburg-Apers et al., 2015). The increased capacity of ciPTEC-OAT1 and -OAT3 to enhance the glycolytic flux is in agreement with the previously observed high extracellular lactate levels in ciPTEC-parent (Figure 1B). This could indicate that the glycolytic flux in these cells is already maximal whereas ciPTEC-OAT1 and -OAT3 have glycolytic spare capacity under basal (i.e. non-inhibited) conditions. This confirms our idea that both ciPTEC-OAT1 and -OAT3 undergo a metabolic shift towards a more oxidative phenotype.

To examine whether the oxidative phenotype was associated with an increased capacity of the electron transferring chain (complexes I–IV), we measured the maximal respiratory capacity of the mitochondrial ETS. Therefore, we first inhibited complex V using oligomycin A, which indicated that the proton leakage (LEAK) from the mitochondrial matrix into the intermembrane space is not different between the three cell lines (Figure 2A). Subsequent titration with the uncoupling agent carbonyl cyanide-4-(trifluoromethoxy)phenylhydrazone (FCCP) demonstrated a similar FCCP sensitivity (Figure S2) and maximal respiratory capacity of the mitochondrial ETS (Figure 2B). This indicates that the increased oxidative phenotype of the ciPTEC-OAT1 and -OAT3 is possibly due to an increased use of the mitochondrial respiratory capacity (Figure 2C), illustrated by a trend towards decreased respiratory reserve capacity in ciPTEC-OAT1 and -OAT3 (47 ± 22% and 58 ± 10%, respectively) compared to ciPTEC-parent (65 ± 16%).

Mitochondrial coupling was stable in all cell lines (Figure 2D), as demonstrated by a comparable mitochondrial membrane potential, visualized by the cationic dye tetramethylrhodamine methyl ester (TMRM). Citrate synthase activity, as measure for mitochondrial content, was determined to confirm that the mitochondrial capacity was unchanged. Indeed, similar activity could be observed in all cell lines, indicating a comparable mitochondrial content in ciPTEC-parent, -OAT1 and -OAT3 (Figure 2E).

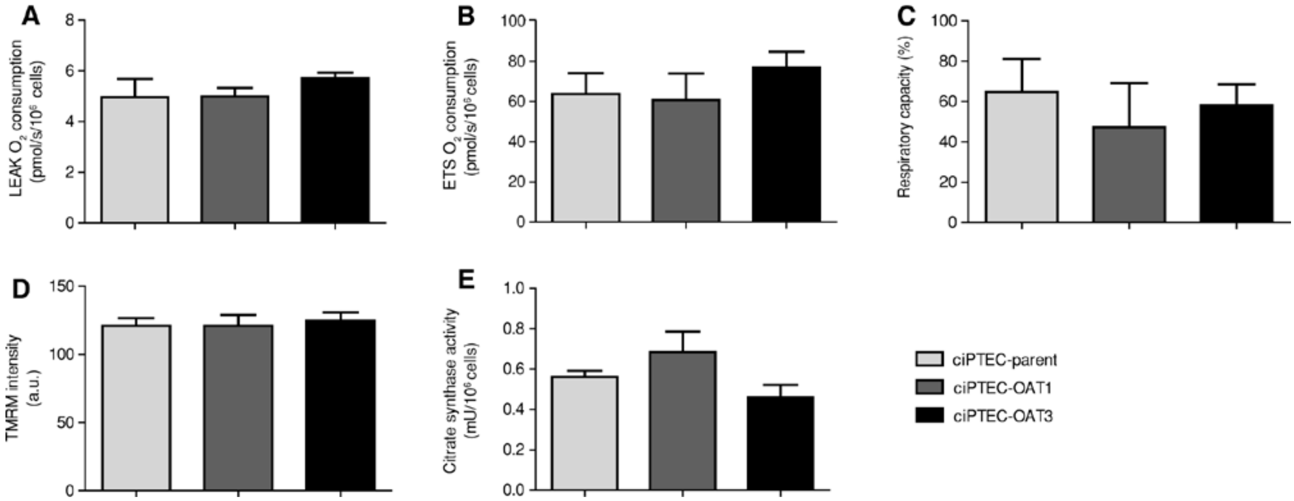

Figure 2: Increased use of mitochondrial respiratory capacity in ciPTEC-OAT1 and -OAT3.
(A) Oxygen consumption measured at proton leakage (LEAK) from mitochondrial matrix into intermembrane space and subsequent (B) titration of FCCP to determine maximal respiratory capacity (ETS). Oxygen consumption at LEAK and ETS was similar in all cell lines. (C) Trend towards decreased respiratory reserve capacities in ciPTEC-OAT1 and -OAT3, possibly indicating increased use of mitochondrial respiratory capacity. (D) Mitochondrial coupling stable in all cell lines, as indicated by a comparable mitochondrial membrane potential visualized by the cationic dye TMRM. (E) Citrate synthase activity, as measure for mitochondrial content, showed similar activities in all cell lines.

To better understand the mechanisms underlying the crosstalk between OAT1 or OAT3 and mitochondrial respiratory rates, we measured TCA cycle metabolites, which have previously been found to be affected in Oat1- or Oat3-deficient mice (Eraly et al., 2006; Wu et al., 2013; Liu et al., 2016). Cellular steady-state levels of TCA cycle metabolites in ciPTEC-parent, -OAT1 and -OAT3 were measured using semi-quantitative liquid chromatography-tandem mass spectrometry (LC-MS/MS) (Figure 3). Interestingly, levels of α-ketoglutarate, a high affinity substrate of OAT1 and OAT3 (Kaufhold et al., 2011), were not significantly decreased (Figure 3B). However, levels of citrate and cis-aconitate, precursors of isocitrate, were decreased in ciPTEC-OAT1 and -OAT3 (Figure 3F, G), and isocitrate itself was significantly lower in ciPTEC-OAT3 (Figure 3H). As all three metabolites are consecutive precursors of α-ketoglutarate in the TCA cycle, this hints towards an increased flux into α-ketoglutarate. This notion is confirmed by the strongly decreased 2-hydroxyglutarate levels in ciPTEC-OAT1 and -OAT3 (Figure 3C), as this metabolite can also be converted into α-ketoglutarate via α-hydroxyacid dehydrogenase (Struys et al., 2007). The latter conversion could also be linked to the increased respiratory rates observed in ciPTEC-OAT1 and -OAT3 (Figure 1C), as electrons released can be transferred to electron-transferring flavoproteins (Engqvist et al., 2014). This can, subsequently, transfer the electrons to coenzyme Q_{10} via electron-transferring flavoprotein dehydrogenase, resulting in an increased reduced status of the coenzyme Q_{10} pool.

The increased efflux of α-ketoglutarate via OAT1 and OAT3 could explain the suggested increased synthesis of α-ketoglutarate in ciPTEC-OAT1 and -OAT3. A similar effect could be observed for succinate, a low affinity substrate of OAT1 and OAT3, as lower levels were found both in ciPTEC-OAT1 and -OAT3, but levels were only significantly reduced in ciPTEC-OAT1 (Figure 3D). Notably, the observed increased synthesis of α-ketoglutarate corresponds to the interaction of TCA cycle metabolites with OAT1 and OAT3 as described *in vivo* and in metabolic network modeling studies (Table 1). To further investigate the role of the dicarboxylates measured here and to understand their origin (either from the TCA cycle or from extracellular sources), we assessed mRNA expression levels of the dicarboxylate cotransporter NaDC3. Gene expression levels of NaDC3 were found to be low in all three cell lines (Table S2), but a significantly higher expression was found in ciPTEC-OAT1. Due to the low expression levels of NaDC3, the measured TCA cycle metabolites most likely originate directly from intracellular sources and not from medium components. This favors our idea that α-ketoglutarate produced by the TCA cycle is upregulated to compensate for the increased efflux by OAT1 and OAT3.

To confirm that the effects on the various TCA cycle metabolites are indeed due to OAT1 and OAT3 transport function, we investigated the effect of OAT inhibition on the levels of TCA cycle metabolites (Figure S3). Exposure of cells to the OAT inhibitor probenecid (100 μM, 24 h), led to decreased levels of α-ketoglutarate and

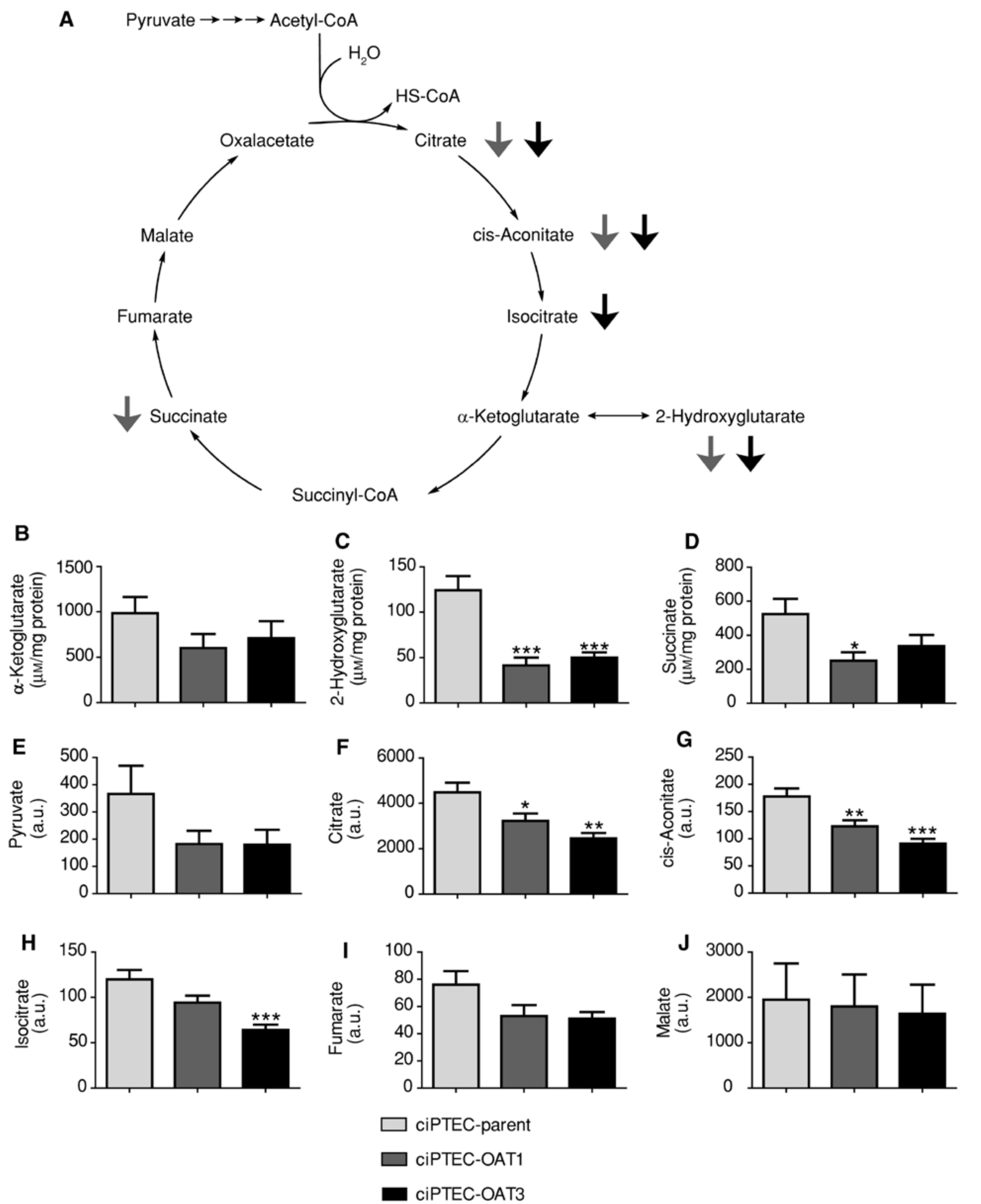

Figure 3: Enhanced flux into α-ketoglutarate synthesis upon OAT overexpression.
(A) Levels of TCA cycle metabolites decreased compared to ciPTEC-parent, as indicated in this schematic overview. Levels of TCA cycle metabolites were measured in ciPTEC-parent, -OAT1 and -OAT3 using semi-quantitative LC-MS/MS. Levels of (B) α-ketoglutarate, (C) 2-hydroxyglutarate and (D) succinate were determined by addition of the corresponding stable isotope, levels of (E) pyruvate, (F) citrate, (G) cis-aconitate, (H) isocitrate, (I) fumarate and (J) malate were determined related to these isotopes. Statistically significant compared to ciPTEC-parent: *$p < 0.05$, **$p < 0.01$, ***$p < 0.001$.

Table 1: Interactions of organic anion transporter 1 and 3 with TCA cycle metabolites and energy metabolism.

Model	Observed effect	Reference
Oat1-deficient mice	Increased urinary excretion of α-ketoglutarate, no significant differences in plasma	Eraly et al., 2006
Oat1-deficient mice and *in vitro* in Oat1-injected *Xenopus* oocytes	Interactions of α-ketoglutarate and fumarate	Ahn et al., 2011
Oat1-deficient mouse combined with *in vitro* data	Interactions of pyruvate, citrate, isocitrate, α-ketoglutarate, succinate, fumarate and malate	Liu et al., 2016
Oat3-deficient mice	No significant changes in levels of α-ketoglutarate in plasma and urine levels	Vallon et al., 2008
Oat3-deficient mice	Decreased urinary excretion of α-ketoglutarate and citrate	Wu et al., 2013
Oat3-deficient mice	No significant changes in plasma levels of TCA cycle metabolites	Bush et al., 2017
Human ciPTEC-OAT1 and -OAT3	Increased synthesis of α-ketoglutarate and metabolic shift towards oxidative phenotype	This study

ciPTEC, Conditionally immortalized proximal tubules epithelial cells; OAT1, organic anion transporter 1; OAT3, organic anion transporter 3; TCA, tricarboxylic acid.

2-hydroxyglutarate in all three cell lines (Figure S3A, B), despite the absence of OAT1 and OAT3 in ciPTEC-parent. As this effect is observed in all cell lines it may relate to off-target effects of probenecid, including inhibition of mitochondrial metabolism (Masereeuw et al., 2000). In general, however, OAT inhibition did not change TCA cycle metabolite levels between ciPTEC-parent, -OAT1 and -OAT3, suggesting that the change in TCA cycle metabolites observed in Figure 3 is inherently associated with the stable expression of OAT1 or OAT3.

Inhibition of OXPHOS will increase levels of NADH and other TCA cycle metabolites, which inhibits the TCA cycle flux and thus α-ketoglutarate production. In addition, α-ketoglutarate is no longer consumed upon OXPHOS inhibition. The resulting condition where α-ketoglutarate is no longer produced and can only be used by OAT1 and OAT3, would lead to further depletion of TCA cycle metabolites (i.e. α-ketoglutarate, citrate, cis-aconitate, isocitrate). Indeed, antimycin A treatment (0.1–10 nM, 24 h) further reduced levels of these TCA cycle metabolites (Figure 4). Levels of α-ketoglutarate were lower in ciPTEC-parent as compared to ciPTEC-OAT1 and -OAT3 (Figure 4B). In comparison to the situation without antimycin A (Figure 3B), this could mean that α-hydroxyacid dehydrogenase was unable to donate its electrons to the electron-transferring flavoproteins due to OXPHOS inhibition, resulting in higher levels of 2-hydroxyglutarate in ciPTEC-OAT1 and -OAT3.

Interestingly, the strong decline of TCA cycle metabolites also observed in ciPTEC-parent may have been due to depletion of most of the metabolites, which efficiently converged into increased succinate levels (Figure 4D). A similar effect could also explain the decreased levels of fumarate and malate in ciPTEC-parent and -OAT1 (Figure 4I, J). It is important to note that the response to antimycin A was similar in ciPTEC-parent and -OAT1, but not in ciPTEC-OAT3 (Figure 4). Levels of pyruvate were not decreased in ciPTEC-OAT3 (Figure 4E), whereas levels of 2-hydroxyglutarate increased (Figure 4C). Furthermore, levels of α-ketoglutarate, fumarate and malate were slightly decreased in ciPTEC-OAT3 compared to vehicle, but higher compared to ciPTEC-parent (Figure 4B, I, J). Together, this indicates that levels of TCA cycle metabolites were less affected by inhibition of mitochondrial respiration in ciPTEC-OAT3 compared to ciPTEC-parent and -OAT1.

In line with the largely depleted α-ketoglutarate levels in all cell lines (Figure 4B) and the indication that this is due to increased α-ketoglutarate efflux, OAT1 and OAT3 transport function should also be largely inhibited upon OXPHOS inhibition. Therefore, uptake of fluorescein, a fluorescent organic anion and substrate of OAT1 and OAT3, was measured after inhibition of cell respiration using mitochondrial inhibitors antimycin A (0.1–10 nM), rotenone (1–200 nM) and myxothiazol (0.1–100 nM) for 24 h (Figure 5A–C). Organic anion transport was markedly reduced upon exposure to antimycin A, rotenone and myxothiazol in both ciPTEC-OAT1 and -OAT3. Direct competition between the mitochondrial complex inhibitors and fluorescein for uptake could be excluded (Figure 5D– F). Inhibitory potencies of the mitochondrial complex inhibitors used on fluorescein uptake (Table S3) were in a similar range as found for the effect on cellular respiration in ciPTEC-OAT1 and -OAT3 (Figure S4, Table S1, S4). Interestingly, the mitochondrial complex III inhibitor myxothiazol had a more potent inhibitory effect on fluorescein uptake via OXPHOS inhibition in ciPTEC-OAT1 compared

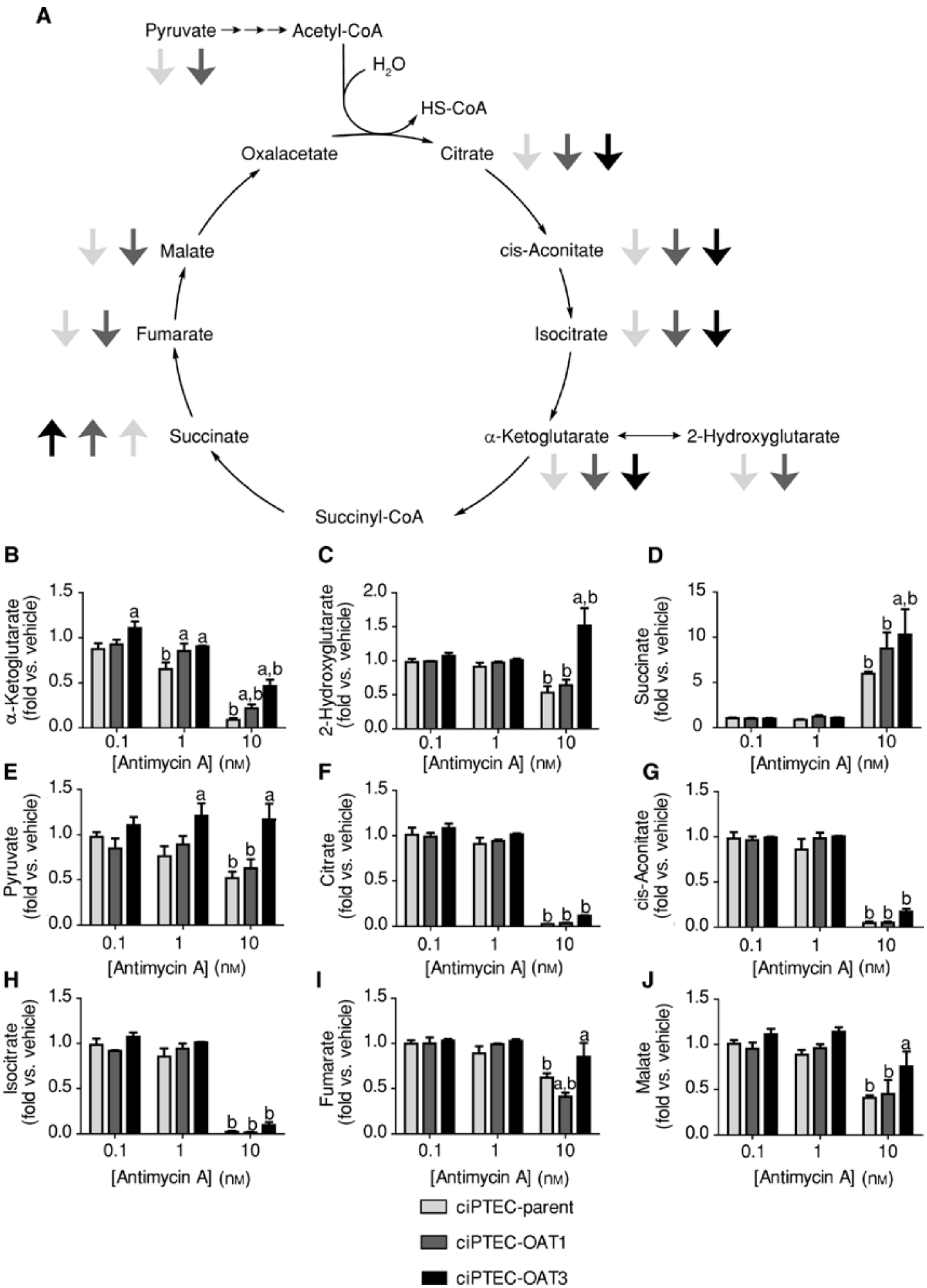

Figure 4: Depletion of TCA cycle metabolites upon inhibition of OXPHOS.
Upon exposure to antimycin A (0.1–10 nM, 24 h) (A) levels of TCA cycle metabolites were depleted and converged into succinate compared to vehicle, as indicated in this schematic overview. Levels of TCA cycle metabolites were measured in ciPTEC-parent, -OAT1 and -OAT3 using semi-quantitative LC-MS/MS. Levels of (B) α-ketoglutarate, (C) 2-hydroxyglutarate (D) succinate were quantified via addition of the corresponding stable isotope. Levels of (E) pyruvate, (F) citrate, (G) cis-aconitate, (H) isocitrate, (I) fumarate and (J) malate were determined related to these isotopes. (B-J) Levels of TCA cycle metabolites are presented as fold difference versus vehicle. Significant differences of means were compared using two-way ANOVA followed by Bonferroni's post-hoc tests. [a]$p < 0.05$ compared to ciPTEC-parent in same condition, [b]$p < 0.05$ compared to corresponding vehicle.

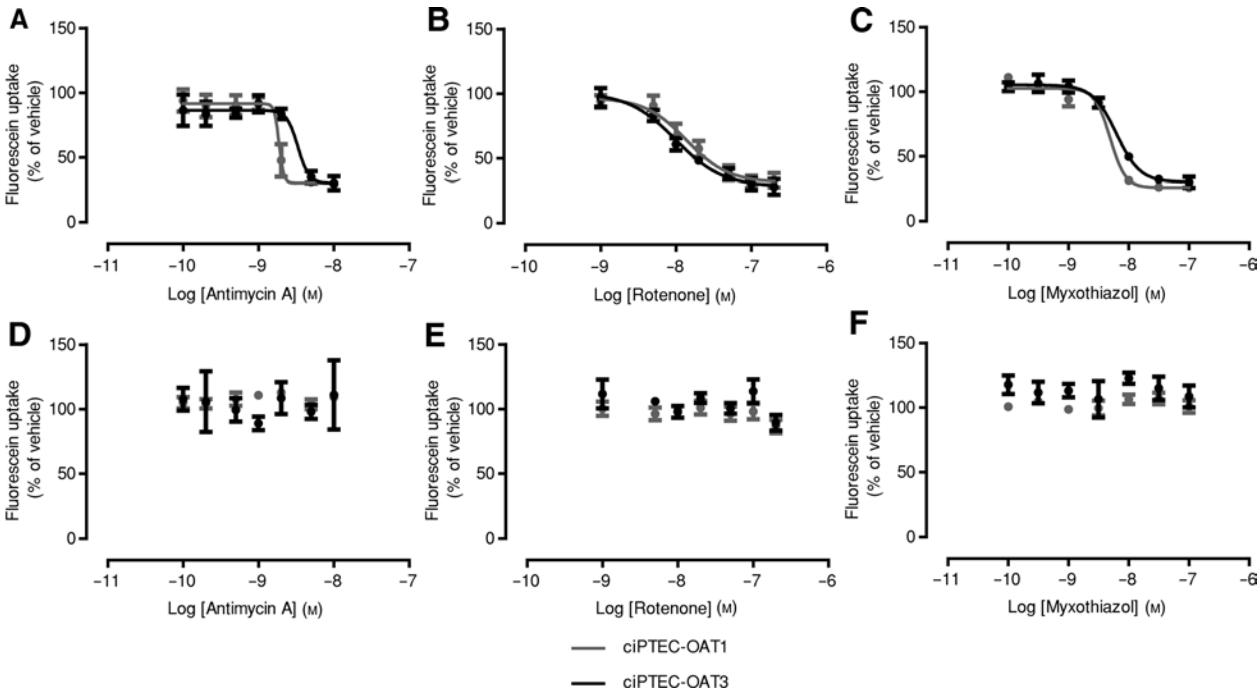

Figure 5: Reduced activity of OAT1 and OAT3 upon inhibition of OXPHOS.
Transport activity determined using fluorescein for ciPTEC-OAT1 (1 µM) and -OAT3 (3 µM), after 24 h exposure to mitochondrial inhibitors (A) antimycin A (0.1–10 nM), (B) rotenone (1–200 nM) or (C) myxothiazol (0.1–100 nM). Dose-dependent decrease in fluorescein uptake. Direct interaction of (D) antimycin A, (E) rotenone or (F) myxothiazol not observed, as determined in presence of these mitochondrial inhibitors at fluorescein uptake.

to -OAT3 (Table S3). These results demonstrate an association between decreased organic anion transport activity and decreased intracellular levels of α-ketoglutarate and other TCA cycle metabolites in ciPTEC-OAT1 and -OAT3, confirming our hypothesized interaction of the OATs and the use of α-ketoglutarate.

Discussion

We demonstrated a shift of energy metabolism in ciPTEC upon OAT1 and OAT3 overexpression towards a more oxidative phenotype, as illustrated by the maintained intracellular ATP levels, but decreased lactate levels compared to ciPTEC-parent. The notion of such a shift was substantiated by elevated basal cellular respiration in ciPTEC-OAT1 and -OAT3. Mitochondrial respiratory inhibition by antimycin A resulted in decreased ATP levels in ciPTEC-parent, but not in -OAT1 and -OAT3. This clearly indicates that ciPTEC-OAT1 and -OAT3 were more capable of maintaining ATP production by increasing glycolysis, as supported by elevated lactate levels. The maintained intracellular ATP levels could be explained by a higher steady-state glucose uptake and subsequent increased glycolytic flux, as previously shown upon antimycin A exposure in C2C12 myoblasts (Liemburg-Apers et al., 2015). In-depth TCA metabolite profiling suggested an increased flux into α-ketoglutarate in ciPTEC-OAT1 and -OAT3, which can be linked to a more reduced status of the coenzyme Q_{10} pool, resulting in higher respiratory rates (i.e. shift towards oxidative phenotype), as schematically illustrated in Figure 6. Experiments using OAT and OXPHOS inhibitors confirmed our idea of increased α-ketoglutarate use and, as a result, increased synthesis in OAT-expressing cells.

Organic anion transport in ciPTEC-OAT1 and -OAT3 was impeded upon OXPHOS inhibition, which is in line with a previous study in OK cells (Nagai et al., 1998). In our study, antimycin A-induced inhibition of OXPHOS had a similar effect on levels of TCA cycle metabolites in ciPTEC-parent and -OAT1, but not in ciPTEC-OAT3. However, the reduced levels of most TCA cycle metabolites, such as α-ketoglutarate, resulted in a starkly decreased uptake of the organic anion fluorescein, in both ciPTEC-OAT1 and -OAT3. Out of a selection of dicarboxylates, α-ketoglutarate showed high affinity for both OAT1 and OAT3 (Kaufhold et al., 2011). Here, we demonstrated that OAT1 activity, but also OAT3 activity, were dependent on levels of TCA cycle metabolites of which α-ketoglutarate seems to provide the clearest association, while the exchange of α-ketoglutarate

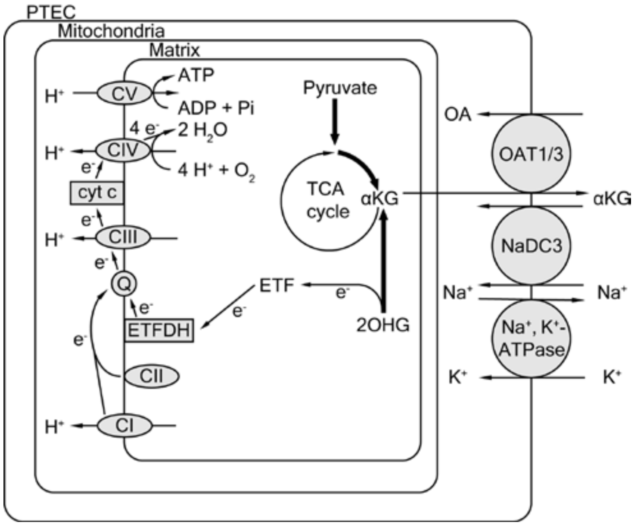

Figure 6: Expression of OAT1 and OAT3 increased the production of α-ketoglutarate.
The TCA cycle and 2-hydroxyglutarate metabolism were increased upon OAT1 and OAT3 expression in PTEC, which resulted in a shift towards a more oxidative phenotype and enhanced α-ketoglutarate production. 2-Hydroxyglutarate can be converted into α-ketoglutarate via α-hydroxyacid dehydrogenase, thereby releasing electrons. These electrons are transferred to coenzyme Q_{10}, via electron-transferring flavoproteins and electron-transferring flavoprotein dehydrogenase, resulting in an increased reduced status of the coenzyme Q_{10} pool and higher respiratory rates. 2OHG, 2-hydroxyglutarate; αKG, α-ketoglutarate; CI, complex I; CII, complex II; CIII, complex III; CIV, complex IV; CV, complex V; cyt c, cytochrome c; e^-, electron; ETF, electron-transferring flavoprotein; ETFDH, electron-transferring flavoprotein dehydrogenase; NaDC3, sodium-dicarboxylate co-transporter 3; OA, organic anion; OAT1/3, organic anion transporter 1/3; PTEC, proximal tubule epithelial cells; Q, coenzyme Q_{10}; TCA, tricarboxylic acid.

in OAT3-mediated organic anion uptake has been questioned before (Bush et al., 2017).

In Oat1-deficient mice, studies of metabolomics revealed a higher urinary excretion of α-ketoglutarate, whereas in Oat3-deficient mice a decreased excretion of α-ketoglutarate was observed (Eraly et al., 2006; Wu et al., 2013; Liu et al., 2016; Bush et al., 2017). Together, these studies demonstrated a pivotal role of OAT1 in energy metabolism in PTEC, while OAT3 was linked to systemic metabolism, mostly in the gut-liver-kidney axis (Liu et al., 2016; Bush et al., 2017). Our *in vitro* metabolomic data correlated with previous studies demonstrating interactions of TCA cycle metabolites with the transporters, studied in Oat1- or Oat3-deficient mice and metabolic reconstructions, as summarized in Table 1. However, these studies focused on plasma and urine levels of metabolites and did not provide information on their intracellular levels. Hence, this study is the first to provide evidence that OAT1 or OAT3 expression affects cellular energy metabolism and synthesis of α-ketoglutarate.

Our work supports a mechanism in which overexpression of OAT1 or OAT3 induces a shift in cellular energy metabolism via an increased metabolite synthesis towards α-ketoglutarate. The role of OAT1 and OAT3 as key components in oxidative metabolism in PTEC has been proposed by others (Eraly et al., 2003; Nigam et al., 2015) and confirmed in the current study. Previously, other intracellular metabolic pathways have also been associated with OAT1 and OAT3 expression, including biosynthesis of amino acids, fatty acids, prostaglandins, cyclic nucleotides and vitamins (Wu et al., 2013; Liu et al., 2016; Bush et al., 2017). The anabolic nature of these metabolic pathways makes their contribution to the observed increased cellular respiration unlikely. These pathways could, however, be changed to compensate for the more oxidative phenotype of the cell. Further studies are needed to investigate whether these pathways are also affected in our ciPTEC-OAT1 -OAT3 cells and how alteration of these various metabolic pathways are associated with each other.

Taken together, this study underlines the important role of organic anion transporters in renal cellular energy metabolism. We demonstrated that energy metabolism in PTEC *in vitro* is more dependent on OXPHOS in cell lines overexpressing OAT1 or OAT3 compared to the isogenic control. Furthermore, transport activity of OAT1 and OAT3 was impeded following OXPHOS inhibition, which could be explained by depletion of TCA cycle metabolites. In conclusion, our results indicate an increased α-ketoglutarate efflux by OAT1 and OAT3, resulting in a metabolic shift towards an oxidative phenotype.

Materials and methods

Compounds and cell culture materials

All compounds used were purchased from Sigma Aldrich (Zwijndrecht, The Netherlands), unless otherwise stated. Cell culture plates were obtained from Greiner Bio-one (Alphen aan den Rijn, The Netherlands).

Cell culture and exposures

Human ciPTEC-parent, ciPTEC-OAT1 and -OAT3 were obtained as described previously (Wilmer et al., 2010; Nieskens et al., 2016). Stable expression and functionality of OAT1 and OAT3 were demonstrated (Nieskens et al., 2016). Cells were cultured at 33°C and 5% (*v/v*) CO_2 to allow proliferation and were used from passage number 35–65 for experiments.

Unless stated otherwise, ciPTEC-parent, -OAT1 and -OAT3 were seeded in 96-well plates at 55 000, 63 000 or 82 000 cells/cm^2, respectively. For cell proliferation, cells were incubated at 33°C and 5% (*v/v*) CO_2 for 1 day to activate the temperature-sensitive mutant of SV large T antigen (SV40T). In order to differentiate the cells into an epithelial monolayer, cells were subsequently cultured for 7 days at 37°C and 5% (*v/v*) CO_2. Cells were cultured in Dulbecco's Modified Eagle Medium (DMEM HAM's F12, Life Technologies, Paisley, UK) supplemented with 5 μg/ml insulin, 5 μg/ml transferrin, 5 μg/ml selenium, 35 ng/ml hydrocortisone (HC), 10 ng/ml epidermal growth factor (EFG), 40 pg/ml tri-iodothyrine (I3), and 10% (*v/v*) fetal calf serum (FCS, Greiner Bio-one), further referred to as PTEC complete medium. Medium was refreshed every 1–2 days.

Stocks of antimycin A, rotenone and myxothiazol were dissolved in absolute ethanol (Merck, Amsterdam, The Netherlands). Probenecid was dissolved in dimethyl sulfoxide (DMSO). Cisplatin was dissolved in PTEC complete medium. Exposures to mitochondrial complex inhibitors antimycin A (0–10 μM), rotenone (0–0.2 μM) and myxothiazol (0–0.1 μM) or OAT-inhibitor probenecid (100 μM) were performed for 24 h on day 6 of maturation, as well for the corresponding vehicles and medium controls. Concentrations of DMSO or ethanol did not exceed 0.1% (*v/v*) or 0.2% (*v/v*), respectively. All experiments were performed on day 7 of maturation.

Levels of intracellular ATP and extracellular lactate

Exposures were performed as described above; exposure to cisplatin (150 μM, 24 h) was used as a positive control. Supernatant from cells was collected after 24 h of exposure and stored at −80°C until measurement. Intracellular ATP was measured immediately after exposures using the ATP bioluminescence assay kit CLS II (Roche, Almere, The Netherlands) following the manufacturer's protocol. Briefly, after 24 h exposure boiling Tris-EDTA buffer [100 mM Tris, 4 mM EDTA (Merck), pH 7.75] was added. Samples were incubated (5 min, 95°C) and centrifuged (5 min, 16 200 *g*, 4°C). Samples were added to a white 96-well plate, diluted in Tris-EDTA buffer (1:1, *v/v*), 30 s after addition of luciferase reagent (1:1, *v/v*) bioluminescence signal was measured on a Victor X3 multiplate reader (Perkin Elmer, Waltham, MA, USA).

To measure extracellular lactate, samples were first diluted (1:10 and 1:20, *v/v*) in MilliQ (MQ), 20 μl of the diluted samples were added to a clear 96-well plate. A dilution series of D-L-lactic acid (60%, *w/w* from syrup) was used as calibration curve. A mixture of glycine (57 mM, Invitrogen, Landsmeer, The Netherlands), hydrazine (145 mM) and NAD^+ grade I (0.88 mM, Roche) at pH 9.5 was added to the samples (1:8, *v/v*) so that total volume was 180 μl per well. Background absorbance was measured at 340 nm on a BioRad microplate spectrophotometer (BioRad, Veenendaal, The Netherlands). Then, 20 μl of L-LDH (Roche) was added at a final concentration of 10 U/ml and incubated for 1 h at room temperature. To determine final concentration of NADH formed, absorbance was measured at 340 nm, and corrected for lactate present in cell culture medium. Levels of ATP and lactate were corrected for mg cellular protein.

High-resolution respiration and citrate synthase activity

Cells were seeded at 55 000 or 40 000 cells/cm^2 in T75 cell culture flasks for cellular respiration measurements and determination of citrate synthase activity. Respiration was measured in thermostated (37°C) chambers of an Oxygraph-2k provided with Datlab 5 recording and analysis software (Oroboros Instruments, Innsbruck, Austria), using $2.0 * 10^6$ cells per chamber. After a stable level of basal respiration was determined (10 min), LEAK from the mitochondrial matrix and respiration at resting level were assessed using complex V inhibitor oligomycin (1 μg/ml). To stimulate uncoupling and to determine maximal capacity of the ETS, a titration was performed using 0.05 μM FCCP per step.

Titrations with rotenone, myxothiazol or antimycin A were performed after reaching stable basal respiration (10 min), titrations with rotenone, myxothiazol or antimycin A were performed until complete inhibition of respiration was observed. For 24 h respiration, cells were treated with antimycin A (10 nM) or corresponding vehicle. Stable basal respiration was determined (10 min).

After all experiments, non-cellular respiration was measured after inhibiting complex I using a final concentration of 0.5 μM rotenone and by inhibiting complex III using a final concentration of 2.5 μM antimycin A.

Citrate synthase activity was measured to determine mitochondrial mass per cell line. Per cell line, $2.0 * 10^6$ cells were harvested and stored at −80°C until further processing. Cell pellet was resuspended in 100 μl ice-cold Tris-HCl (Invitrogen, Carlsbad, CA, USA) buffer (10 mM pH 7.6) and pottered. Homogenate was added to a new vial with sucrose (Acros Organics, Bleiswijk, The Netherlands) (250 mM) and was centrifuged (10 min, 600 *g*, 4°C) to remove cell debris. Supernatant was collected, subsequently centrifuged (10 min, 14 000 *g*, 4°C) to isolate mitochondrial fraction and resuspended in 150 μl Tris-HCl. Citrate synthase activity was measured spectrophotometrically, as earlier described (Janssen et al., 2006).

Cell viability and mitochondrial membrane potential

Cells were seeded in black/clear flat bottom 96-well plates (Corning, Amsterdam, The Netherlands), cultured and exposed as described already. For cell viability, nuclei, necrotic and apoptotic cells were stained for 20 min at 37°C using Hoechst33342 (20 μg/ml, Life Technologies), propidium iodide (1 μg/ml) and YO-PRO-1 (2 μM, Life Technologies), respectively. Images were acquired using a 10× objective Becton Dickinson (BD) Pathway 855 high-throughput microscope (BD Bioscience, Breda, The Netherlands). Images were analyzed using Fiji (version 1.51n) (Schindelin et al., 2012). Hoechst images were counted and then used as mask to determine propidium iodide and YO-PRO-1 positive cells. Cell viability was calculated as percentage of propidium iodide and YO-PRO-1-stained cells compared to total nuclei count.

To determine mitochondrial membrane potential, cells were stained with 25 nM TMRM (Life Technologies) and Hoechst33342 (20 μg/ml) for 30 min at 37°C. Images were acquired using a 40× objective on a BD Pathway 855. TMRM images were corrected for background and uneven illumination and were then analyzed by masking a binarized image for mitochondrial area using Image Pro Plus 6.3 software (Media Cybernetics, Silver Spring, MD, USA), as previously described (Koopman et al., 2005).

Gene expression

CiPTEC-parent, -OAT1 and -OAT3 were seeded in 6-well plates at 60 000, 55 000 or 32 000 cells/cm^2, respectively. RNA extraction was performed using the RNeasy Mini Kit (Qiagen, Venlo, The Netherlands). Complementary DNA (cDNA) was obtained via Moloney Murine Leukemia Virus (M-MLV, Invitrogen) reverse transcriptase following the manufacturer's protocol. Gene expression levels of *GAPDH* (hs99999905_m1), *HPRT1* (hs02800695_m1), HIF1α (*HIF1A*, hs00153153_m1) and *SLC13A3* (hs00955744_m1) were quantified using gene-specific primer-probe sets and TaqMan Universal polymerase chain reaction (PCR) Master mix from Applied Biosystems (Bleiswijk, The Netherlands). Quantitative PCR reactions were measured using CFX96-Touch Real-Time PCR System (BioRad) and analyzed with BioRad CFX Manager (version 3.1). GADPH was used as a reference gene.

TCA cycle metabolites

Levels of TCA cycle metabolites were determined using semi-quantitative LC-MS/MS. Cells (6-well plates) were exposed to antimycin A or probenecid, washed twice with ice-cold Hanks' Balanced Salt Solution (HBSS, Life Technologies) and incubated with 1 ml absolute methanol (LC-MS grade) (Boom, Meppel, The Netherlands) for 5 min on ice. Cells were harvested using a plastic scraper, samples were centrifuged (10 min, 1500 *g*, 4°C), and supernatant was collected and stored at −80°C until measurement. Prior to measurement, methanol was evaporated. The extracts were redissolved by adding 20 μl of 4% (*w/w*) formic acid, 100 μl of d4-α-ketoglutarate (Cambridge Isotope Laboratories, Buchem, Apeldoorn, The Netherlands) (2 μM in H_2O), 10 μl of $^{13}C_5$-2-hydroyxglutarate (Chiralix, Nijmegen, The Netherlands) (9 μM in H_2O) and 50 μl of d4-succinate (Cambridge Isotope Laboratories) (3 μM in H_2O) and passed through a 30 kDa centrifugal filter (30 min, 14 000 *g*, 15°C). Five microliters of the filtrate were injected into the HPLC-MS/MS system consisting of a Waters I-Class Acquity (Breda, The Netherlands) fitted with a peek-lined InertSustain AQ-c18 (GL Sciences, Eindhoven, The Netherlands) (2.1*100 mm dp 3 μ) column connected to a Waters Xevo TQSμ mass spectrometer. The column was run at 40°C in gradient mode using 0.5% (*v/v*) acetic acid in H_2O and acetonitrile (VWR, Amsterdam, The Netherlands), with initial conditions 100% acetic acid (0.5%, *v/v*) in H_2O at 250 μl/min. The column flow was directed to the Xevo TQSμ fitted with an electrospray ionization probe operating in the negative mode at unit resolution. The capillary voltage was set at 0.6 kV. The temperature settings for the source and ion block were 550°C and 150°C, respectively. As a drying gas nitrogen was used at a flow rate of 800 l/h. The cone gas flow was set at 50 l/h. The collision cell was operated with argon as the collision gas at a pressure of 0.35 Pa. An area response of the TCA cycle metabolites of interest was recorded using retention time depending multiple reaction monitoring (MRM) transitions. α-Ketoglutarate, 2-hydroxyglutarate and succinate were quantified using their added corresponding stable isotope. The other TCA cycle metabolites, lacking an added stable isotope, could not be quantified. Their area response was merely normalized and reported in arbitrary units. All levels were corrected for mg cellular protein.

Fluorescein uptake

Activity of OAT1 and OAT3, in ciPTEC-OAT1 or -OAT3, was measured as previously described (Nieskens et al., 2016). Cells were exposed to fluorescein for OAT1 (1 μM) and OAT3 (3 μM) after exposure (direct or 24 h) to mitochondrial complex inhibitors.

Data and statistical analysis

Statistical tests were performed using GraphPad Prism version 5.03 (San Diego, CA, USA). Data is presented as mean ± SEM of at least three independent experiments (n = 3). Unless stated otherwise, means were considered to be statistically significant different if $p < 0.05$ using one-way analysis of variance (ANOVA) followed by Dunnett's multiple comparison post-hoc test. For fluorescein uptake and respiration titration of mitochondrial inhibitors, after background subtraction, data was normalized to activity of untreated control cells or basal respiration, respectively. Inhibition curves were plotted as log (concentrations of mitochondrial complex inhibitor) versus fluorescein uptake or respiration in GraphPad Prism. Data was fitted with non-linear regression with variable slope constraining the bottom to >0.

Acknowledgments: This project was supported by the NephroTube project funded by the National Center for the Replacement, Refinement and Reduction of Animals in Research (NC3Rs), Funder Id: 10.13039/501100000849, under the Crack-it challenge 15 (Nephrotube) project no. 37497–25920. The authors thank Werner J. Koopman and Peter H. Willems (Department of Biochemistry, Radboud University Medical Center, Nijmegen, The Netherlands) for their input and advice regarding this study. The authors would also like to thank the microscopic imaging center at Radboud University Medical Center for using the imaging facilities.

Conflict of interest statement: M.J. Wilmer and F.G.M. Russel are co-inventors on patent EP2010/066792 'Novel conditionally immortalized human proximal tubule cell line expressing functional influx and efflux transporters' assigned to Radboud University Medical Center and as such M.J. Wilmer and F.G.M. Russel have a conflict of interest through the commercialization of ciPTEC models via Cell4Pharma.

References

Ahn, S.Y., Jamshidi, N., Mo, M.L., Wu, W., Eraly, S.A., Dnyanmote, A., Bush, K.T., Gallegos, T.F., Sweet, D.H., Palsson, B.O., et al. (2011). Linkage of organic anion transporter-1 to metabolic pathways through integrated "omics"-driven network and functional analysis. J. Biol. Chem. *286*, 31522–31531.

Brandt, U., Schagger, H., and von Jagow, G. (1988). Characterisation of binding of the methoxyacrylate inhibitors to mitochondrial cytochrome c reductase. Eur. J. Biochem. *173*, 499–506.

Bush, K.T., Wu, W., Lun, C., and Nigam, S.K. (2017). The drug transporter oat3 (slc22a8) and endogenous metabolite communication via the gut-liver-kidney axis. J. Biol. Chem. *292*, 15789–15803.

Engqvist, M.K., Esser, C., Maier, A., Lercher, M.J., and Maurino, V.G. (2014). Mitochondrial 2-hydroxyglutarate metabolism. Mitochondrion *19*, 275–281.

Eraly, S.A., Blantz, R.C., Bhatnagar, V., and Nigam, S.K. (2003). Novel aspects of renal organic anion transporters. Curr. Opin. Nephrol. Hypertens. *12*, 551–558.

Eraly, S.A., Vallon, V., Vaughn, D.A., Gangoiti, J.A., Richter, K., Nagle, M., Monte, J.C., Rieg, T., Truong, D.M., Long, J.M., et al. (2006). Decreased renal organic anion secretion and plasma accumulation of endogenous organic anions in oat1 knock-out mice. J. Biol. Chem. *281*, 5072–5083.

Fedecostante, M., Westphal, K.G.C., Buono, M.F., Sanchez Romero, N., Wilmer, M.J., Kerkering, J., Baptista, P.M., Hoenderop, J.G., and Masereeuw, R. (2018). Recellularized native kidney scaffolds as a novel tool in nephrotoxicity screening. Drug Metab. Dispos. *46*, 1338–1350.

Janssen, A.J., Trijbels, F.J., Sengers, R.C., Wintjes, L.T., Ruitenbeek, W., Smeitink, J.A., Morava, E., van Engelen, B.G., van den Heuvel, L.P., and Rodenburg, R.J. (2006). Measurement of the energy-generating capacity of human muscle mitochondria: diagnostic procedure and application to human pathology. Clin. Chem. *52*, 860–871.

Kaufhold, M., Schulz, K., Breljak, D., Gupta, S., Henjakovic, M., Krick, W., Hagos, Y., Sabolic, I., Burckhardt, B.C., and Burckhardt, G. (2011). Differential interaction of dicarboxylates with human sodium-dicarboxylate cotransporter 3 and organic anion transporters 1 and 3. Am. J. Physiol. Renal Physiol. *301*, F1026–1034.

Koopman, W.J., Verkaart, S., Visch, H.J., van der Westhuizen, F.H., Murphy, M.P., van den Heuvel, L.W., Smeitink, J.A., and Willems, P.H. (2005). Inhibition of complex I of the electron transport chain causes $O^{2-\cdot}$-mediated mitochondrial outgrowth. Am. J. Physiol. Cell Physiol. *288*, C1440–1450.

Liemburg-Apers, D.C., Schirris, T.J., Russel, F.G., Willems, P.H., and Koopman, W.J. (2015). Mitoenergetic dysfunction triggers a rapid compensatory increase in steady-state glucose flux. Biophys. J. *109*, 1372–1386.

Liu, H.C., Jamshidi, N., Chen, Y., Eraly, S.A., Cho, S.Y., Bhatnagar, V., Wu, W., Bush, K.T., Abagyan, R., Palsson, B.O., et al. (2016). An organic anion transporter 1 (oat1)-centered metabolic network. J. Biol. Chem. *291*, 19474–19486.

Masereeuw, R., van Pelt, A.P., van Os, S.H., Willems, P.H., Smits, P., and Russel, F.G. (2000). Probenecid interferes with renal oxidative metabolism: a potential pitfall in its use as an inhibitor of drug transport. Br. J. Pharmacol. *131*, 57–62.

Nagai, J., Yano, I., Hashimoto, Y., Takano, M., and Inui, K. (1998). Efflux of intracellular alpha-ketoglutarate via *p*-aminohippurate/dicarboxylate exchange in ok kidney epithelial cells. J. Pharmacol. Exp. Ther. *285*, 422–427.

Nieskens, T.T., Peters, J.G., Schreurs, M.J., Smits, N., Woestenenk, R., Jansen, K., van der Made, T.K., Roring, M., Hilgendorf, C., Wilmer, M.J., et al. (2016). A human renal proximal tubule cell line with stable organic anion transporter 1 and 3 expression predictive for antiviral-induced toxicity. AAPS J. *18*, 465–475.

Nigam, S.K., Wu, W., Bush, K.T., Hoenig, M.P., Blantz, R.C., and Bhatnagar, V. (2015). Handling of drugs, metabolites, and uremic toxins by kidney proximal tubule drug transporters. Clin. J. Am. Soc. Nephrol. *10*, 2039–2049.

O'Connor, P.M. (2006). Renal oxygen delivery: Matching delivery to metabolic demand. Clin. Exp. Pharmacol. Physiol. *33*, 961–967.

Pagliarini, D.J., Calvo, S.E., Chang, B., Sheth, S.A., Vafai, S.B., Ong, S.E., Walford, G.A., Sugiana, C., Boneh, A., Chen, W.K., et al. (2008). A mitochondrial protein compendium elucidates complex I disease biology. Cell *134*, 112–123.

Peters, E., Schirris, T., van Asbeck, A.H., Gerretsen, J., Eymael, J., Ashikov, A., Adjobo-Hermans, M.J., Russel, F., Pickkers, P., and Masereeuw, R. (2017). Effects of a human recombinant alkaline phosphatase during impaired mitochondrial function in human renal proximal tubule epithelial cells. Eur. J. Pharmacol. *796*, 149–157.

Pritchard, J.B. (1988). Coupled transport of p-aminohippurate by rat kidney basolateral membrane vesicles. Am. J. Physiol. *255*, F597–604.

Schindelin, J., Arganda-Carreras, I., Frise, E., Kaynig, V., Longair, M., Pietzsch, T., Preibisch, S., Rueden, C., Saalfeld, S., Schmid, B., et al. (2012). Fiji: an open-source platform for biological-image analysis. Nat. Methods *9*, 676–682.

Shimada, H., Moewes, B., and Burckhardt, G. (1987). Indirect coupling to na+ of p-aminohippuric acid uptake into rat renal basolateral membrane vesicles. Am. J. Physiol. *253*, F795–801.

Struys, E.A., Gibson, K.M., and Jakobs, C. (2007). Novel insights into l-2-hydroxyglutaric aciduria: Mass isotopomer studies reveal 2-oxoglutaric acid as the metabolic precursor of l-2-hydroxyglutaric acid. J. Inherit. Metab. Dis. *30*, 690–693.

Suter-Dick, L., Mauch, L., Ramp, D., Caj, M., Vormann, M.K., Hutter, S., Lanz, H.L., Vriend, J., Masereeuw, R., and Wilmer, M.J. (2018). Combining extracellular mirna determination with microfluidic 3d cell cultures for the assessment of nephrotoxicity: a proof of concept study. AAPS J. *20*, 86.

Vallon, V., Eraly, S.A., Wikoff, W.R., Rieg, T., Kaler, G., Truong, D.M., Ahn, S.Y., Mahapatra, N.R., Mahata, S.K., Gangoiti, J.A., et al. (2008). Organic anion transporter 3 contributes to the regulation of blood pressure. J. Am. Soc. Nephrol. *19*, 1732–1740.

Vriend, J., Nieskens, T.T.G., Vormann, M.K., van den Berge, B.T., van den Heuvel, A., Russel, F.G.M., Suter-Dick, L., Lanz, H.L., Vulto, P., Masereeuw, R., et al. (2018). Screening of drug-transporter interactions in a 3d microfluidic renal proximal tubule on a chip. AAPS J. *20*, 87.

Wikoff, W.R., Nagle, M.A., Kouznetsova, V.L., Tsigelny, I.F., and Nigam, S.K. (2011). Untargeted metabolomics identifies enterobiome metabolites and putative uremic toxins as substrates of organic anion transporter 1 (oat1). J. Proteome. Res. *10*, 2842–2851.

Wilmer, M.J., Saleem, M.A., Masereeuw, R., Ni, L., van der Velden, T.J., Russel, F.G., Mathieson, P.W., Monnens, L.A., van den Heuvel, L.P., and Levtchenko, E.N. (2010). Novel conditionally immortalized human proximal tubule cell line expressing functional influx and efflux transporters. Cell Tissue Res. *339*, 449–457.

Wu, W., Jamshidi, N., Eraly, S.A., Liu, H.C., Bush, K.T., Palsson, B.O., and Nigam, S.K. (2013). Multispecific drug transporter slc22a8 (oat3) regulates multiple metabolic and signaling pathways. Drug Metab. Dispos. *41*, 1825–1834.

Wu, W., Bush, K.T., and Nigam, S.K. (2017). Key role for the organic anion transporters, oat1 and oat3, in the *in vivo* handling of uremic toxins and solutes. Sci. Rep. *7*, 4939.

Supplementary Material: The online version of this article offers supplementary material (https://doi.org/10.1515/hsz-2018-0446).